Polymer Chemistry

ROYAL SOCIETY OF CHEMISTRY

PAPER

View Article Online
View Journal | View Issue

Cite this: *Polym. Chem.*, 2020, **11**, 3716

Precise tracking and modulating aggregation structures of conjugated copolymers in solutions†

Zi-Yuan Wang,[a] Ze-Fan Yao,[a] Yang Lu,[a] Li Ding,[a] Zi-Di Yu,[a] Hao-Yang You,[a] Xin-Yi Wang,[a] Yang-Yang Zhou,[a] Lin Zou,*[b] Jie-Yu Wang[a] and Jian Pei *[a]

Received 28th March 2020,
Accepted 6th May 2020

DOI: 10.1039/d0py00456a

rsc.li/polymers

The effects of the backbone shape of the conjugated polymers on the aggregation features in solutions, and further on the morphology in solid states are rarely reported. Herein, four copolymers, BDOPV-T, BDOPV-$T_{0.8}$-$2T_{0.2}$, BDOPV-$T_{0.2}$-$2T_{0.8}$, and BDOPV-2T, are developed to reveal that the aggregation structures of these polymers are dependent on the special properties of the conjugated backbone. Our investigation demonstrates that the aggregation microstructures of these polymers in solid states are inheritable from those in solutions.

Introduction

The aggregation structures of conjugated polymers in solutions have exhibited great influence on the performance of solution-processed devices, such as organic field-effect transistors (OFETs),[1–3] organic photovoltaics (OPVs)[4–6] and organic thermoelectrics (OTEs).[7–10] Some homopolymers usually aggregated in solutions, and at some points, such aggregates showed consistency with their thin film morphology.[11–13] For instance, octyl-substituted polyfluorenes aggregated into a rod-like structure in toluene.[14] Polythiophene-based polymers adopted a random coil geometry in solutions as the alkyl chains were modified.[15] However, unlike these homopolymers, donor–acceptor (D–A) conjugated polymers exhibit stronger and more complex interchain interactions, and might form complicated aggregation structures even in dilute solutions.[16,17] Therefore, it remains a challenge to investigate the aggregation mechanisms and the structures of D–A conjugated polymers in solutions.[18–22]

In our previous report, we found that the backbone shape of isoindigo-based conjugated polymers affected their packing modes in thin films, and further led to different charge mobilities in OFETs.[23] Subsequently, several D–A conjugated polymers also showed the similar results.[24,25] However, few investigations on the relationship between molecular structures and the aggregation mechanisms and the structures in solutions were explored systematically. Herein, we develop four copolymers, BDOPV-T, BDOPV-$T_{0.8}$-$2T_{0.2}$, BDOPV-$T_{0.2}$-$2T_{0.8}$, and BDOPV-2T, in which the conformation of the polymer backbones converts from wavy to linear structures as the ratio of bithiophene units increased. We analysed the specific aggregation structures of these four copolymers in solutions to associate with the molecular backbone shape. The study roadmap from molecular shape, solution-state aggregation structures, thin-film microstructures, finally to electron mobility and doping efficiency is well-focused. In dilute solutions, BDOPV-T and BDOPV-$T_{0.8}$-$2T_{0.2}$ with the wavy backbones, adopt random coil structures, while polymers BDOPV-$T_{0.2}$-$2T_{0.8}$ and BDOPV-2T with the linear backbones, form 1D worm-like structures. Higher electron mobilities could be achieved from the thin films spin-casted of BDOPV-$T_{0.2}$-$2T_{0.8}$ and BDOPV-2T. In contrast, polymers with random coil aggregates in solutions could be more easily doped with the n-dopant. For the first time, we demonstrate that higher doping efficiency could be obtained due to the random coil aggregation structures in solutions even though the intrinsic charge carrier mobility of BDOPV-T and BDOPV-$T_{0.8}$-$2T_{0.2}$ polymers is lower, which might further contribute to comparable conductivities to those of BDOPV-$T_{0.2}$-$2T_{0.8}$ and BDOPV-2T. Overall, the investigations from the backbone shape, to the aggregation structures in solution, and then to the thin film microstructures, finally to device performance are initially built up.

[a]*Beijing National Laboratory for Molecular Sciences (BNLMS), Key Laboratory of Polymer Chemistry and Physics of Ministry of Education, Center of Soft Matter Science and Engineering, College of Chemistry and Molecular Engineering, Peking University, Beijing 100871, China. E-mail: jianpei@pku.edu.cn*
[b]*Institute of Nuclear Physics and Chemistry, China Academy of Engineering Physics, Mianyang 621999, China. E-mail: jurling@pku.edu.cn*

†Electronic supplementary information (ESI) available. See DOI: 10.1039/d0py00456a

Results and discussion

Synthesis and materials

Scheme 1 illustrates the synthetic approach to the monomers and the desired polymers. All monomers were synthesized following the previous reported procedures.[26] The Stille polymer-

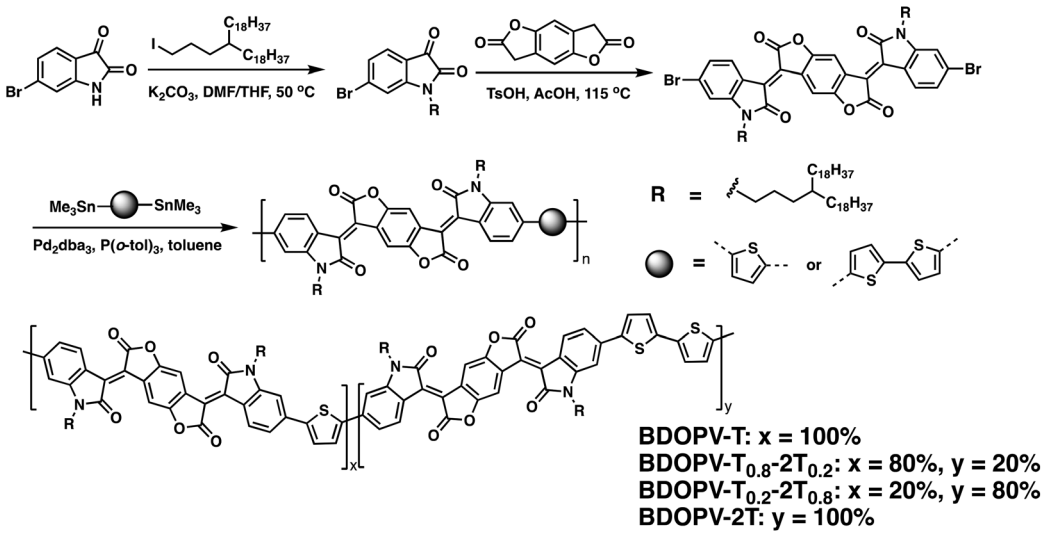

Scheme 1 Synthesis route and molecular structures of four BDOPV-based polymers.

ization of BDOPV (benzodifurandione-based oligo(*p*-phenylene vinylene))-based dibromide, 2,5-bis(trimethylstannyl)thiophene (T) and 5,5′-bis(trimethylstannyl)-2,2′-bithiophene (2 T) in different molar proportions was employed to give four copolymers, BDOPV-T, BDOPV-$T_{0.8}$-$2T_{0.2}$, BDOPV-$T_{0.2}$-$2T_{0.8}$, and BDOPV-2T, respectively. These four polymers were purified through precipitation by adding methanol, followed by Soxhlet extraction using acetone, hexanes, and then chloroform. High-temperature gel permeation chromatography (GPC) with 1,2,4-trichlorobenzene as the eluent gave the molecular weights of polymers (BDOPV-T: M_n = 31.4 kDa, polydispersity index (PDI) = 1.6; BDOPV-$T_{0.8}$-$2T_{0.2}$: M_n = 33.4 kDa, PDI = 2.6; BDOPV-$T_{0.2}$-$2T_{0.8}$: M_n = 35.8 kDa, PDI = 2.4; BDOPV-2T: M_n = 38.5 kDa, PDI = 3.4). The ratios of thiophene and bithiophene units in BDOPV-$T_{0.8}$-$2T_{0.2}$ and BDOPV-$T_{0.2}$-$2T_{0.8}$ polymers could be confirmed by using X-ray photoelectron spectroscopy (XPS) (Fig. S1†). XPS measurements demonstrated that the ratios between thiophene and bithiophene units were in line with our design. For instance, the ratio of peaks at 400 eV (wherein the nitrogen atoms in BDOPV motifs) and around 164 eV (wherein the sulfur atoms in thiophene and bithiophene units) was 1.44 in BDOPV-$T_{0.8}$-$2T_{0.2}$, which is consistent with the theoretical value (1.36). This measurement is also suitable for BDOPV-$T_{0.2}$-$2T_{0.8}$ polymers (the relative errors are given in Table S1†). The backbone shape of the four polymers was characterized by using quantum calculation and molecular dynamics. BDOPV-T exhibited a typical wavy structure, while BDOPV-2T showed a linear structure (Fig. 1a and b). All the polymers exhibited excellent thermal stability with decomposition temperatures of >370 °C (Fig. S2a†). A phase transition around 20 °C was observed for all the polymers, regardless of polymer backbone structures (Fig. S2b–S2e†).

Optical and electrochemical properties

Ultraviolet–visible-near infrared (UV-*vis*-NIR) absorption spectra and cyclic voltammetry (CV) measurements were performed on these polymers. Their absorption spectra both in 1,2-dichlorobenzene (*o*-DCB) solution and in thin films are shown in Fig. 1c and d. Table 1 summarizes the basic photophysical and electrochemical properties of these polymers. All polymers (BDOPV-T, BDOPV-$T_{0.8}$-$2T_{0.2}$, BDOPV-$T_{0.2}$-$2T_{0.8}$, and BDOPV-2T) showed characteristic absorption band around 600–1000 nm, with the optical gaps of 1.39 eV, 1.36 eV, 1.34 eV, 1.32 eV, respectively. Clearly, the absorption onset showed significant red-shift as the ratio of bithiophene units increased, which was due to the more extended effective conjugation length along the more linear backbones.[27] Meanwhile, the absorption features of their thin films were almost consistent with those in solutions (Fig. 1d), which demonstrated that the rigid backbone or the aggregation behaviors of these polymers formed in solutions. Varied-temperature absorption spectra of four polymer solutions (Fig. S3†) showed a slightly blue-shift as the solution temperature increased, which might also indicate the distortion and disaggregation of the four polymers in solutions.[19,28]

The electrochemical properties of the four polymers in thin films were investigated by CV measurements (Fig. S4† and Table 1). The ionization potential (IP) values gradually decreased from 5.79 eV to 5.47 eV as the gradual dominating of bithiophene units. In contrast, the electron affinity (EA) values, remained almost the same of about 4.0 eV. It could be well-understood by the theoretical computation, which revealed that the electron density of LUMO levels mainly localized on the BDOPV motifs in the four polymers (Fig. S5†).

Aggregates in solutions and solid states

In view of their strong aggregation behaviors in solutions, small-angle neutron scattering (SANS) measurements were performed to elucidate the aggregation structures of the four polymers.[29,30] For BDOPV-T and BDOPV-$T_{0.8}$-$2T_{0.2}$ in d_4-*o*-DCB solutions, the $I(q)$–q curves fitted best with the random coil model (Fig. 2a and d).[30] According to the Zimm plot

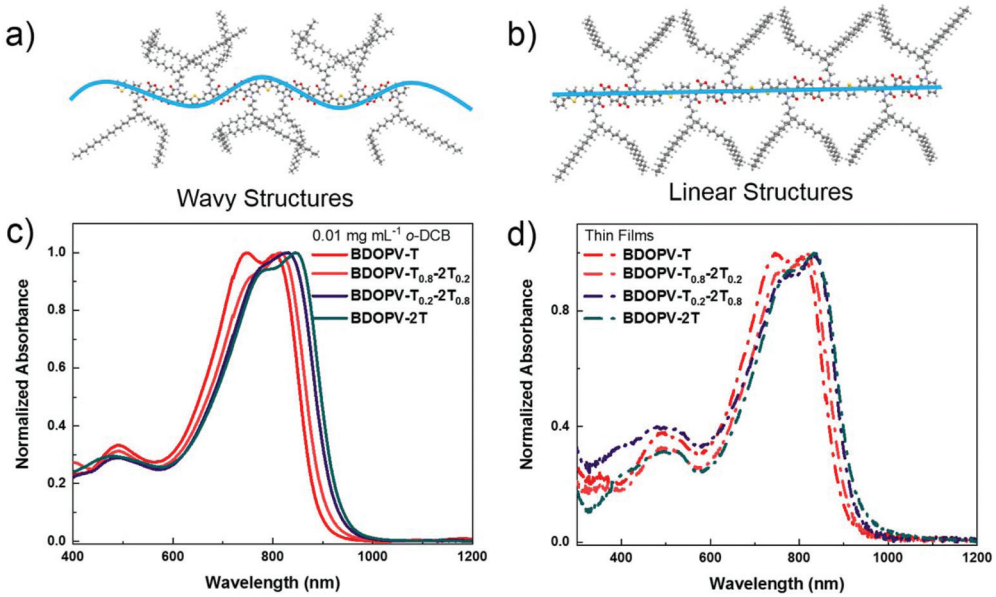

Fig. 1 (a and b) The minimum energy conformations of tetramers of BDOPV-T and BDOPV-2T, which were optimized with Dreiding force field; (c and d) UV-*vis*-NIR absorption spectra of intrinsic polymer solutions and thin films, respectively.

Table 1 Molecular weight, optical and electrochemical properties of four copolymers with different ratio of thiophene and bithiophene units

Polymer	M_n (kDa)/PDI	λ_{max} [a] (nm)	λ_{max} [b] (nm)	E_g^{opt} (eV)	IP^{CV} (eV)	EA^{CV} (eV)
BDOPV-T	31.4/1.6	747, 805	750, 805	1.39	5.79	4.09
BDOPV-$T_{0.8}$-$2T_{0.2}$	33.4/2.6	815	816	1.36	5.73	4.08
BDOPV-$T_{0.2}$-$2T_{0.8}$	35.8/2.4	831	832	1.34	5.63	3.98
BDOPV-2T	38.5/3.4	847	833	1.32	5.47	4.00

[a] 0.01 mg mL^{-1} *o*-DCB polymer solutions. [b] Thin film states.

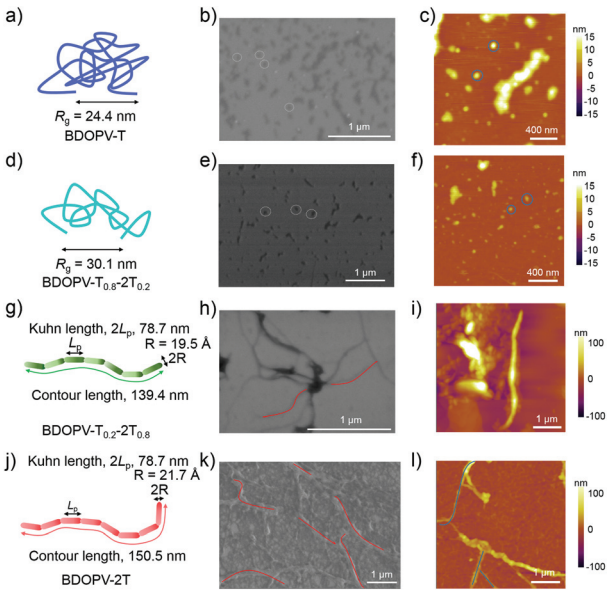

Fig. 2 Aggregation models obtained from SANS data of BDOPV-T (a), BDOPV-$T_{0.8}$-$2T_{0.2}$ (d), BDOPV-$T_{0.2}$-$2T_{0.8}$ (g) and BDOPV-2T (j) in d_4-*o*-DCB solution (a) and (d) only represented one aggregation chain; AFM height images, SEM images of BDOPV-T (b and c), BDOPV-$T_{0.8}$-$2T_{0.2}$ (e and f), BDOPV-$T_{0.2}$-$2T_{0.8}$ (h and i) and BDOPV-2T (k and l) after freeze-drying.

($1/I$ *vs.* Q^2), which is widely used in the light scattering of dilute polymer solutions,[30] we could yield an important factor – the radius of gyration. In this model, the mean-squared radius of gyration (R_g) is the main parameter to describe the extent of polymers chain folding.[29] Larger R_g represented less folding of polymers.[31] The R_gs of BDOPV-T and BDOPV-$T_{0.8}$-$2T_{0.2}$ were calculated to be 243.8 Å and 301.1 Å, respectively. Compared with BDOPV-T, BDOPV-$T_{0.8}$-$2T_{0.2}$ exhibited less folded chain conformation, which revealed that embedding bithiophene units would progressively unfold the molecular chain, leading to a large R_g.

With increasing the ratio of bithiophene motif, the scattering data of BDOPV-$T_{0.2}$-$2T_{0.8}$ and BDOPV-2T were substantially different (Fig. 2g and j). Their aggregation structures could be best described using the worm-like chain model,[19,31] which is in good agreement with 1D structure inferred from Porod exponent (Fig. S6†).[32] The worm-like chain model is widely used to describe semi-rigid chains, which is a common model for π-conjugated polymers. In the worm-like chain model, the contour length (L_{ct}), Kuhn length ($2L_p$, L_p represents the persistence length) and radius (R) are three important parameters to describe the conformation of polymer chain.[19] The contour length suggested the polymer chain length at maximum physically possible extension, and the Kuhn length could characterize the stiffness of a given polymer chain. According to the worm-like model, L_{ct} of BDOPV-$T_{0.2}$-$2T_{0.8}$ was 139.4 nm, and the Kuhn length ($2L_p$) were calculated to be 78.7 nm. Meanwhile, L_{ct} of BDOPV-2T was 150.5 nm, and the Kuhn

length ($2L_p$) were calculated to be 78.7 nm. Surprisingly, the contour lengths of the two polymers were much longer than their length of a single polymer chain (≈53 nm, see the ESI†), suggesting that in d_4-*o*-DCB, BDOPV-$T_{0.2}$-$2T_{0.8}$ and BDOPV-2T adopted 1D worm-like aggregation structures due to their strong interchain π–π stacking. Also, BDOPV-2T formed larger aggregates than BDOPV-$T_{0.2}$-$2T_{0.8}$. The Kuhn length of BDOPV-$T_{0.2}$-$2T_{0.8}$ felled between the total length of thirty-nine repeating units of BDOPV-T and thirty-two repeating units of BDOPV-2T. The Kuhn length of BDOPV-2T equalled to the length of thirty-two repeating units. These results indicated the stiffness of the polymer backbones in the solution state due to the strong intramolecular hydrogen bonding. Compared with the random coil aggregates of BDOPV-T and BDOPV-$T_{0.8}$-$2T_{0.2}$, the 1D worm-like aggregates originated from stronger interchain interactions might be beneficial to charge carrier transport of polymers and have a negative impact on mixing with dopants.

Freeze drying is a direct means to transfer the aggregation structures in solution to the solid state.[33–35] The characterization of the freeze-dried states of these four polymers was performed by atomic force microscopy (AFM) and scanning electron microscopy (SEM). Due to the π–π interactions, the random coil of polymers would wrap with each other, resulting in a spherical structure. As a result, BDOPV-T aggregates (Fig. 2b) in *o*-DCB solution displayed a spherical shape with diameters of 30–70 nm, which agreed with the radius of gyration measured from SANS data. The AFM height images showed that the aggregate sizes were larger than the SANS results, which was likely due to the further aggregation upon removing the solvent (Fig. 2c). Polymer BDOPV-$T_{0.8}$-$2T_{0.2}$ also aggregated into a spherical structure with diameters of 40–100 nm, and AFM images illustrated the similar results with those of BDOPV-T (Fig. 2e and f).

As the bithiophene units dominating, BDOPV-$T_{0.2}$-$2T_{0.8}$ and BDOPV-2T showed apparent 1D worm-like structures in SEM and AFM images. The length of BDOPV-$T_{0.2}$-$2T_{0.8}$ aggregates ranged from 60 to 300 nm (Fig. 2h and i), which was well consistent with the contour length from SANS. For BDOPV-2T, much larger aggregates than BDOPV-$T_{0.2}$-$2T_{0.8}$ were observed in SEM images. These results revealed that in freezing *o*-DCB solution, aggregates of BDOPV-T and BDOPV-$T_{0.8}$-$2T_{0.2}$ adopted spherical structures, while the behaviors of BDOPV-$T_{0.2}$-$2T_{0.8}$ and BDOPV-2T were compliance with 1D worm-like model. The spatial sizes of the polymer aggregates observed from SEM and AFM further clearly proved that BDOPV-$T_{0.8}$-$2T_{0.2}$ owned a less folded structure than BDOPV-T. Moreover, the contour length of BDOPV-2T was significantly longer than that of BDOPV-$T_{0.2}$-$2T_{0.8}$, indicating the stronger interchain interactions in BDOPV-2T.

Furthermore, thin films of four polymers spin-coated from *o*-DCB solutions were fabricated to investigate the relationship between solution-state aggregation structures and solid-state microstructures. For the thin films of BDOPV-T and BDOPV-$T_{0.8}$-$2T_{0.2}$, the AFM height images showed smooth surfaces and small aggregates, while the thin films of BDOPV-$T_{0.2}$-$2T_{0.8}$ and BDOPV-2T exhibited large aggregates and intercalating networks with surface root-mean-square (RMS) around 1 nm (Fig. 3e–h). Grazing-incidence wide-angle X-ray scattering (GIWAXS) measurements were performed on

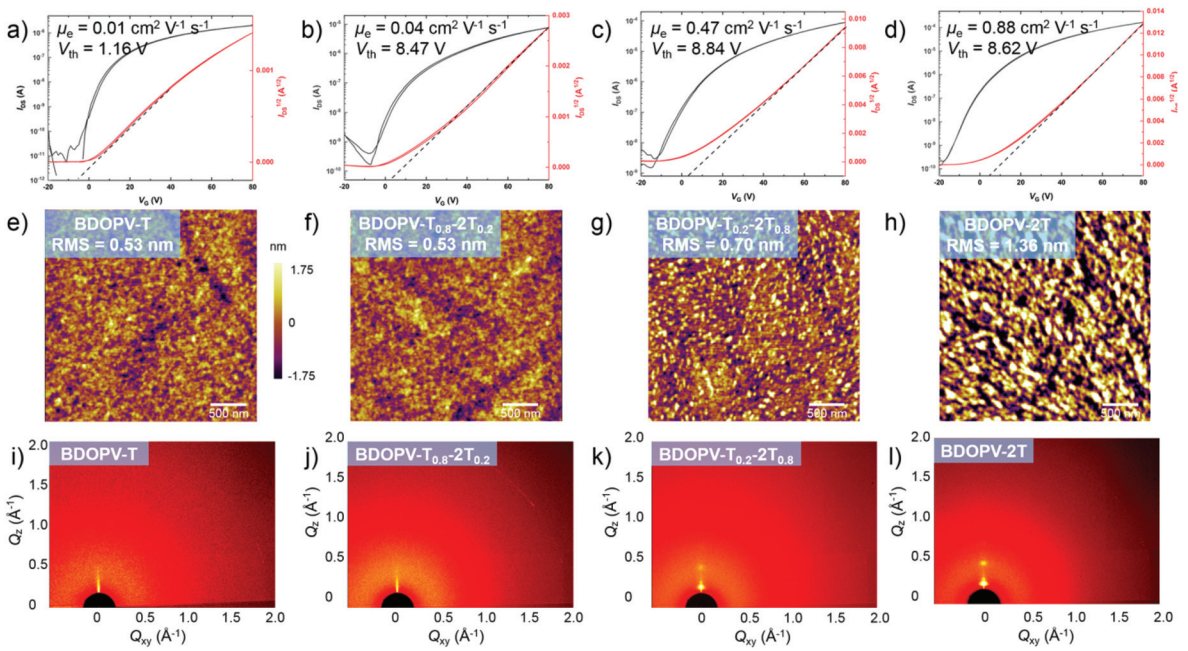

Fig. 3 (a–d) Representative transfer characteristics of thin film transistors based on BDOPV-T, BDOPV-$T_{0.8}$-$2T_{0.2}$, BDOPV-$T_{0.2}$-$2T_{0.8}$ and BDOPV-2T, respectively. (e–h) AFM height images of thin films of BDOPV-T, BDOPV-$T_{0.8}$-$2T_{0.2}$, BDOPV-$T_{0.2}$-$2T_{0.8}$ and BDOPV-2T. (i–l) 2D GIWAXS patterns of BDOPV-T, BDOPV-$T_{0.8}$-$2T_{0.2}$, BDOPV-$T_{0.2}$-$2T_{0.8}$ and BDOPV-2T thin films.

four conjugated polymer films (Fig. 3i–l and S7†). From the 2D GIWAXS patterns and 1D plots, obvious (100), (200) diffraction peaks could be observed along the out-of-plane direction in BDOPV-$T_{0.2}$-$2T_{0.8}$ and BDOPV-2T polymer films. Usually, coherence length is adopted to reflect the size of crystalline domains. In 1D GIWAXS plots, larger coherence length of BDOPV-$T_{0.2}$-$2T_{0.8}$ and BDOPV-2T illustrated that both of them had higher crystallinity (Table S2†). However, the thin films of BDOPV-T and BDOPV-$T_{0.8}$-$2T_{0.2}$ showed an almost negligible diffraction signal in both in-plane and out-of-plane directions and smaller coherence length. These results indicated the low crystallinity and amorphous morphology of BDOPV-T and BDOPV-$T_{0.8}$-$2T_{0.2}$. Therefore, we established the relationship between molecular backbone shape and aggregation structures in solution – the wavy BDOPV-based polymers adopted random coil aggregates in solution state, while the linear polymers showed 1D worm-like aggregates and these aggregates would further inherit into the thin films.

Charge transport properties

To evaluate the charge transport properties of these four copolymers, OFET devices with top-gate/bottom-contact (TG/BC) configuration were fabricated. All the copolymers have displayed n-type transport behaviors. With increasing the ratio of bithiophene units in polymers, the electron mobilities increased gradually (Fig. 3a–d, S8 and Table S3†). BDOPV-2T showed the highest average electron mobility of 0.84 ± 0.29 $cm^2 V^{-1} s^{-1}$, almost two orders of magnitude higher than BDOPV-T polymers. The average carrier mobilities of BDOPV-$T_{0.2}$-$2T_{0.8}$, BDOPV-$T_{0.8}$-$2T_{0.2}$ and BDOPV-T were 0.50 ± 0.06 $cm^2 V^{-1} s^{-1}$, 0.06 ± 0.01 $cm^2 V^{-1} s^{-1}$ and 0.01 ± 0.002 $cm^2 V^{-1} s^{-1}$, respectively. The differences in carrier mobilities indicated that the aggregates of these conjugated polymers in solutions indeed played a critical role in determining their solid-stated microstructures, further influencing the charge transport properties.

Doping efficiency and conductive properties

Based on the above studies, we speculated that the random coil aggregation states of BDOPV-T and BDOPV-$T_{0.8}$-$2T_{0.2}$ in solutions would be doped more easily due to the weaker interchain interactions compared to BDOPV-$T_{0.2}$-$2T_{0.8}$ and BDOPV-2T. Therefore, we mixed various molar ratios of (4-(1,3-dimethyl-2,3-dihydro-1*H*-benzimidazol-2-yl)phenyl)dimethylamine (*N*-DMBI) with these four polymers to investigate their doping process and conductive properties (Fig. S9†). UV-*vis*-NIR measurements were performed to monitor the doping process (Fig. 4a, b and S10, S11†). After adding the same ratio (24 mol%) of the dopant (*N*-DMBI) into the polymer solutions, the absorption bands of BDOPV-T and BDOPV-$T_{0.8}$-$2T_{0.2}$ at near-infrared region were lifted more obviously than those of BDOPV-$T_{0.2}$-$2T_{0.8}$ and BDOPV-2T, which suggested that the doping efficiency of BDOPV-T and BDOPV-$T_{0.8}$-$2T_{0.2}$ polymers were higher than BDOPV-$T_{0.2}$-$2T_{0.8}$ and BDOPV-2T in solutions. Moreover, thin films of the four doped polymers were obtained through direct drying in the glove box under the same conditions. The thin film absorption spectra of BDOPV-T and BDOPV-$T_{0.8}$-$2T_{0.2}$ also featured stronger absorbance in the near-infrared region. These results indicated that the aggregation states in doped solution could also be inherited into the thin film states under the doping process.

Moreover, we analysed the film morphologies of these four copolymers after doping by AFM as shown in Fig. 4 and S12.† Under the lower doping concentration (≈24 mol%), the surface

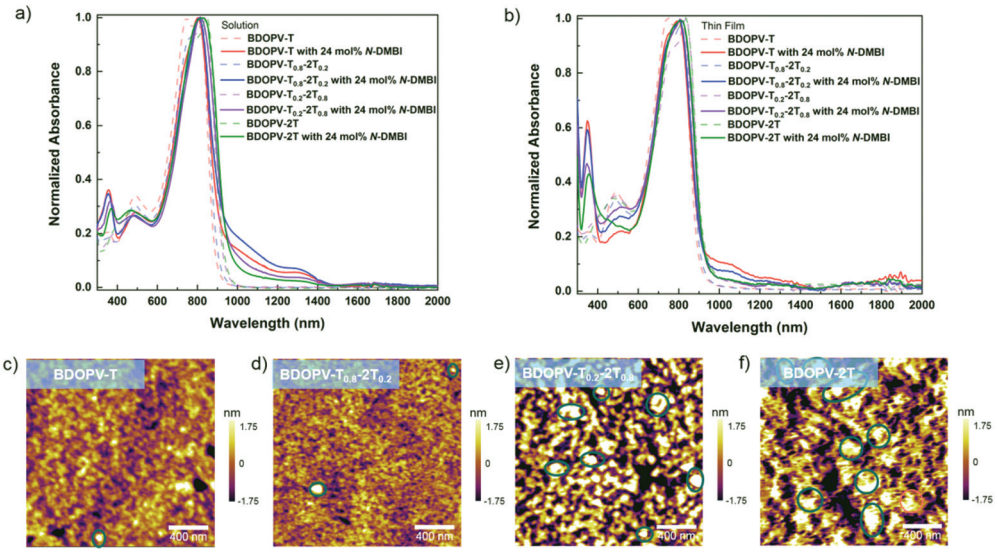

Fig. 4 (a) Normalized UV-*vis*-NIR absorption spectra of the intrinsic and 24 mol% doped solution of BDOPV-T, BDOPV-$T_{0.8}$-$2T_{0.2}$, BDOPV-$T_{0.2}$-$2T_{0.8}$ and BDOPV-2T; (b) normalized thin-film UV-*vis*-NIR absorption spectra of the intrinsic and 24 mol% doped BDOPV-T, BDOPV-$T_{0.8}$-$2T_{0.2}$, BDOPV-$T_{0.2}$-$2T_{0.8}$ and BDOPV-2T. (c–f) AFM height images of BDOPV-T, BDOPV-$T_{0.8}$-$2T_{0.2}$, BDOPV-$T_{0.2}$-$2T_{0.8}$ and BDOPV-2T doped with 48 mol% *N*-DMBI.

roughness of BDOPV-T and BDOPV-$T_{0.8}$-$2T_{0.2}$ almost unchanged due to the excellent miscibility of polymers with *N*-DMBI, illustrating the effective mixing between the host polymers and dopant molecules. Further increasing the dopant concentration, it could be observed that small spherical aggregates were dispersed on the polymer films. Compared with BDOPV-T and BDOPV-$T_{0.8}$-$2T_{0.2}$, BDOPV-2T and BDOPV-$T_{0.2}$-$2T_{0.8}$ displayed more aggregates under the same dopant concentration (Fig. 4e and f), verifying the poor miscibility of the polymer hosts with the dopant molecules. In addition, current–voltage measurements were performed on the four doped polymer films with various molar ratios of *N*-DMBI (Fig. S14†). A maximal conductivity of 0.07 S cm^{-1} and 0.12 S cm^{-1} after *N*-DMBI doping could be obtained in BDOPV-T and BDOPV-$T_{0.8}$-$2T_{0.2}$. Meanwhile, the maximal conductivities of BDOPV-$T_{0.2}$-$2T_{0.8}$ and BDOPV-2T were 0.2 S cm^{-1} and 0.04 S cm^{-1}, respectively. These results suggested that polymers BDOPV-$T_{0.2}$-$2T_{0.8}$ and BDOPV-2T with more linear backbone shape were difficult to be doped, while wavy polymers BDOPV-T and BDOPV-$T_{0.8}$-$2T_{0.2}$ were more easily doped with *N*-DMBI.

Conclusions

In summary, we have demonstrated that the different backbone shape of the BDOPV-based polymers exhibited a distinct relationship with aggregation structures in solution, and then further led to different charge transport properties and doping efficiency of these polymers. The polymers with the wavy backbone shape tend to aggregate into random coil structures, while the linear polymers form 1D worm-like structures in solution. Moreover, the random coil aggregates in solution state had weaker interchain interactions, but were more easily doped, leading to higher carrier concentrations and comparable conductivities. In comparison, stronger interchain interactions and better charge transport properties could be obtained from polymers showing 1D worm-like aggregates in solution, but they were hard to be uniformly mixed with dopants. Our results provide a deep understanding to the relationship between the molecular design and aggregation structures in solution for high-performance organic field-effect transistors, photovoltaics and thermoelectrics.

Author contributions

Z.-Y. W designed and carried out the experiments, analyzed the data and wrote the manuscript. Z.-F. Y and Y. L played a critical role in the discussion of the experimental design, project direction. L. D, Z.-D. Y, X.-Y. W and Y.-Y. Z collected the UV-*vis*-NIR, CV, AFM, OFET and conductivity data. H.-Y. Y gave the discussion on the preparation of the manuscript. All the authors discussed the results and commented on the manuscript.

Conflicts of interest

There are no conflicts to declare.

Acknowledgements

This work is supported by National Key R&D Program of China (2017YFA0204701), National Natural Science Foundation of China (21790360, 21722201). The authors acknowledge the High-Performance Computing Platform of Peking University for supporting the computational work. The authors thank beamline BL14B1 at Shanghai Synchrotron Radiation Facility for providing the beam time.

Notes and references

1 Z. C. Chen, M. G. Li, M. X. Hu, S. Wang, Z. G. Miao, S. Xu, C. L. Chen, H. L. Dong, W. Huang and R. F. Chen, *J. Mater. Chem. C*, 2020, **8**, 2094–2101.
2 C. B. Nielsen, M. Turbiez and I. McCulloch, *Adv. Mater.*, 2013, **25**, 1859–1880.
3 L. Ding, Z.-Y. Wang, J.-Y. Wang and J. Pei, *Chin. J. Chem.*, 2020, **38**, 13–24.
4 J. Lee, E. S. Shin, Y. J. Kim, Y. Y. Noh and C. Yang, *J. Mater. Chem. C*, 2020, **8**, 296–302.
5 N. Zhang, Y. X. Xu, X. B. Zhou, W. Zhang, K. Zhou, L. M. Yu, W. Ma and X. F. Xu, *J. Mater. Chem. C*, 2019, **7**, 14130–14140.
6 X. J. Wang, Y. D. Yang, Z. C. He, H. B. Wu and Y. Cao, *J. Mater. Chem. C*, 2019, **7**, 14861–14866.
7 Y. Lu, J. Y. Wang and J. Pei, *Chem. Mater.*, 2019, **31**, 6412–6423.
8 B. Russ, A. Glaudell, J. J. Urban, M. L. Chabinyc and R. A. Segalman, *Nat. Rev. Mater.*, 2016, **1**, 16050.
9 Y. Lu, Z.-D. Yu, R.-Z. Zhang, Z.-F. Yao, H.-Y. You, L. Jiang, H.-I. Un, B.-W. Dong, M. Xiong, J.-Y. Wang and J. Pei, *Angew. Chem., Int. Ed.*, 2019, **58**, 11390–11394.
10 K. Shi, F. Zhang, C.-A. Di, T.-W. Yan, Y. Zou, X. Zhou, D. Zhu, J.-Y. Wang and J. Pei, *J. Am. Chem. Soc.*, 2015, **137**, 6979–6982.
11 S. P. O. Danielsen, T.-Q. Nguyen, G. H. Fredrickson and R. A. Segalman, *ACS Macro Lett.*, 2019, **8**, 88–94.
12 E. Lim, A. M. Glaudell, R. Miller and M. L. Chabinyc, *Adv. Electron. Mater.*, 2019, 1800915.
13 L. Verheyen, K. Janssens, M. Marinelli, E. Salatelli and G. Koeckelberghs, *Macromolecules*, 2019, **52**, 6578–6584.
14 M. Knaapila, V. M. Garamus, F. B. Dias, L. Almásy, F. Galbrecht, A. Charas, J. Morgado, H. D. Burrows, U. Scherf and A. P. Monkman, *Macromolecules*, 2006, **39**, 6505–6512.
15 B. McCulloch, V. Ho, M. Hoarfrost, C. Stanley, C. Do, W. T. Heller and R. A. Segalman, *Macromolecules*, 2013, **46**, 1899–1907.
16 Y. Q. Zheng, T. Lei, J. H. Dou, X. Xia, J. Y. Wang, C. J. Liu and J. Pei, *Adv. Mater.*, 2016, **28**, 7213–7219.

17 Y. Xi, C. M. Wolf and L. D. Pozzo, *Soft Matter*, 2019, **15**, 1799–1812.
18 M. Li, C. An, T. Marszalek, M. Baumgarten, H. Yan, K. Mullen and W. Pisula, *Adv. Mater.*, 2016, **28**, 9430–9438.
19 Y.-Q. Zheng, Z.-F. Yao, T. Lei, J.-H. Dou, C.-Y. Yang, L. Zou, X. Meng, W. Ma, J.-Y. Wang and J. Pei, *Adv. Mater.*, 2017, **29**, 1701072.
20 Y. Liu, J. Zhao, Z. Li, C. Mu, W. Ma, H. Hu, K. Jiang, H. Lin, H. Ade and H. Yan, *Nat. Commun.*, 2014, **5**, 5293.
21 M. Li, H. Bin, X. Jiao, M. M. Wienk, H. Yan and R. A. J. Janssen, *Angew. Chem.*, 2020, **59**, 846–852.
22 P. Wan, C. B. An, T. Zhang, K. Q. Ma, N. N. Liang, Y. Xu, S. Q. Zhang, B. W. Xu, J. Q. Zhang and J. H. Hou, *Polym. Chem.*, 2020, **11**, 1629–1636.
23 T. Lei, Y. Cao, X. Zhou, Y. Peng, J. Bian and J. Pei, *Chem. Mater.*, 2012, **24**, 1762–1770.
24 M. Wang, M. J. Ford, C. Zhou, M. Seifrid, T. Q. Nguyen and G. C. Bazan, *J. Am. Chem. Soc.*, 2017, **139**, 17624–17631.
25 R. Rieger, D. Beckmann, A. Mavrinskiy, M. Kastler and K. Müllen, *Chem. Mater.*, 2010, **22**, 5314–5318.
26 T. Lei, J.-H. Dou, X.-Y. Cao, J.-Y. Wang and J. Pei, *Adv. Mater.*, 2013, **25**, 6589–6593.
27 T. Lei, Y. Cao, Y. Fan, C.-J. Liu, S.-C. Yuan and J. Pei, *J. Am. Chem. Soc.*, 2011, **133**, 6099–6101.
28 Z.-F. Yao, Y.-Q. Zheng, Q.-Y. Li, T. Lei, S. Zhang, L. Zou, H.-Y. Liu, J.-H. Dou, Y. Lu, J.-Y. Wang, X. Gu and J. Pei, *Adv. Mater.*, 2019, **31**, 1806747.
29 Y. B. Melnichenko and G. D. Wignall, *J. Appl. Phys.*, 2007, **102**, 021101.
30 B. Hammouda, *Polym. Rev.*, 2010, **50**, 14–39.
31 I. Teraoka, *Polymer Solutions: An Introduction to Physical Properties*, Wiley, New York, 2002.
32 P. d. L. Iglesia and D. C. Pozzo, *Soft Matter*, 2013, **9**, 11214.
33 N. Thongprachan, K. Nakagawa, N. Sano, T. Charinpanitkul and W. Tanthapanichakoon, *Mater. Chem. Phys.*, 2008, **112**, 262–269.
34 Y.-J. Jin, W.-E. Lee, C.-L. Lee and G. Kwak, *Soft Matter*, 2016, **12**, 4443–4448.
35 S. Sambashivan, Y. Liu, M. R. Sawaya, M. Gingery and D. Eisenberg, *Nature*, 2005, **437**, 266–269.